Solar Energy Vol. 36, No. 6, pp. 481–497, 1986
Printed in the U.S.A.

0038–092X/86 $3.00 + .00

AN ANISOTROPIC HOURLY DIFFUSE RADIATION MODEL FOR SLOPING SURFACES: DESCRIPTION, PERFORMANCE VALIDATION, SITE DEPENDENCY EVALUATION

R. Perez†, R. Stewart†, C. Arbogast, R. Seals, J. Scott†
Atmospheric Sciences Research Center, State University of New York at Albany, 1400 Washington Avenue, Albany, New York 12222

(*Received* 31 *May* 1985; *accepted* 7 *November* 1985)

Abstract—A model is described to estimate hourly or higher frequency diffuse sky radiation impinging on plane surfaces of any orientation, once knowing this value on the horizontal. This model features a simple geometrical sky hemisphere description, allowing for the observed effects of forward-scattered and back-scattered radiation and a parameterization of insolation conditions based on available radiative quantities.

Model performance is studied through (1) long term independent tests performed against hourly ground-shielded tilted irradiance data from Trappes, France; Carpentras, France and San Antonio, Texas; (2) long term dependent tests performed against hourly data from the same stations plus Albany, New York; and (3) real time tests based on one-minute data from Albany, New York. Performance is assessed through comparison with three reference models: the isotropic, the Hay, and Klucher anisotropic models. Substantial performance improvement over the three reference models is found for all stations and all surface orientations. Additional performance improvements from independent to dependent testing can be explained logically on the basis of climate, altitude and latitude differences between stations.

1. INTRODUCTION

As solar energy system modeling became more refined over the last ten years, the requirements for input radiation parameters became more demanding. Both accurate radiation data bases and adequate models are in increasing need by the engineering community worldwide. The current undertaking of the International Energy Agency in this field[1] is an illustration of this specific interest.

Notably, the hourly modeling of the energy received by tilted planes, based on the knowledge of horizontal global radiation and normal incidence direct radiation, is of prime importance. The anisotropic nature of diffuse radiation has been the largest source of error associated with this computation. Many authors have pointed out the shortcomings of the classical isotropic assumption, e.g., [2, 3], and recent photovoltaic projects in the United States have demonstrated the need for better models in this area[4].

However, there exist today, several models which attempt to account for diffuse radiation anisotropy. The most successful have been observed to better the isotropic model in many instances, e.g., [5, 6, 7].

The model described and tested in this paper was developed as an attempt to improve systematically on the isotropic assumption for all weather conditions and all captor orientations, by using (1) a simple, realistic geometric representation of radiance distribution within the sky hemisphere; (2) a sky-condition description scheme making full use of the information already available to compute hourly irradiance on slopes, i.e., global horizontal, direct and/or diffuse, position of the sun; and (3) an experimentally-derived law governing the relationship between sky condition and radiance distribution. This model will be subsequently referred to as *Perez model*.

2. METHODS

2.1 *Description of the Perez model*

The model is composed of three distinct elements: (1) A geometrical representation of the sky dome, (2) A parametric representation of the insolation conditions, and (3) A statistical component linking the two.

2.1.1 *The geometrical framework.* This is represented in Fig. 1, where the sky hemisphere is divided into three zones. Radiance originating from each of these regions can be different, while remaining constant within a given zone. Such a configuration was decided upon in order to account for the two main zones of anisotropy observed in the

† Member ISES.

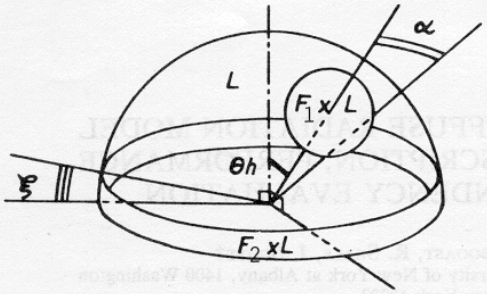

Fig. 1. Model geometrical representation of the sky hemisphere.

atmosphere: circumsolar brightening, due to forward scattering by aerosols, and horizon brightening due primarily to multiple Rayleigh scattering and retroscattering in clear atmospheres[10].

If the radiances originating from the main portion of the dome, the circumsolar, and the horizon zone are respectively equal to L, $F_1 \times L$, and $F_2 \times L$, the resulting horizontal diffuse irradiance Dh can be expressed as

$$Dh = \pi L\{1 + 2(1 - \cos\alpha)Xh(z)(F_1 - 1)\cos z' + 0.5(1 - \cos 2\xi)(F_2 - 1)\}, \quad (1)$$

where α is the half angle of the circular region centered on the sun's position and set at 15° for the model studied here. The parameter Xh is the fraction of this circular region which is seen by the horizontal, while the angle z' is equal to the solar zenith angle, z, if the circular region is totally visible, and equal to its average incidence angle if it is only partially visible. The angle ξ is the horizon band angular thickness, set at 6.5° for the presented model.

Equation (1) assumes that the circumsolar region is small enough so that all points within this region are seen under the same angle, z'.

Similarly the diffuse irradiance, Dc, received by a sloping plane is expressed as

$$Dc = \pi L\{0.5(1 + \cos s) + 2(1 - \cos\alpha)Xc(\theta)(F_1 - 1)\cos\theta' + 2\xi \sin\xi'(F_2 - 1)/\pi\}, \quad (2)$$

where s is the plane's tilt angle, while the angles θ and θ' and the parameter Xc are the equivalent of z, z', and Xh respectively, for the considered surface.

The last term of eqn (2) is a sinusoidal approximation of the horizon band contribution to the energy budget of the plane, where the angle ξ' is defined as

$$\xi' = s + \xi(\tfrac{1}{2} - s/\pi). \quad (3)$$

This approximation causes a minor deviation from the actual integrated value[11] and generates a slight discontinuity for $s = 0$; however, its effect is negligible when placed in the operating model context.

The combination of eqns (1) and (2) leads to the model's governing equation

$$Dc = Dh\{0.5(1 + \cos s) + a(\theta)(F_1 - 1) + b(s)(F_2 - 1)\}\{1 + c(z)(F_1 - 1) + d(F_2 - 1)\}^{-1}, \quad (4)$$

where

$$a(\theta) = 2(1 - \cos\alpha)Xc(\theta)\cos\theta', \quad (5)$$

$$b(s) = 2\xi \sin\xi'/\pi, \quad (6)$$

$$c(z) = 2(1 - \cos\alpha)Xh(z)\cos z', \quad (7)$$

$$d = (1 - \cos 2\xi)/2. \quad (8)$$

Equation (4) is identical to the isotropic equation for $F_1 = F_2 = 1$.

2.1.2 *The sky condition parameterization.* Considering that the calculation of irradiance on a slope at a given instant requires the knowledge of the normal incidence direct irradiance, the horizontal diffuse irradiance, and the solar position, it is logical to use that information to describe the type of sky condition existing at that instant. The three following variables are used for this purpose:

- z, solar zenith angle
- Dh, horizontal diffuse radiation
- $\varepsilon = (Dh + I)/Dh$, where I is the normal incidence direct.

It is assumed, at this stage of model development, that z, Dh and ϵ are independent quantities defining a 3-dimensional space. This space is divided into over 200 "sky condition categories," by defining intervals for each of the variables. These are presented in Table 1.

2.1.3 *The sky condition/model configuration relationship.* The only undefined terms in eqns (1) and (2) are the coefficients F_1 and F_2. These non-dimensional multiplicative factors set the radiance magnitude in the two anisotropic regions relatively to that in the main portion of the dome. The degree of anisotropy of the model is a function of these two terms only. The model can go from an isotropic configuration (F_1, $F_2 = 1$) to a configuration incorporating circumsolar and/or horizon brightening.

The magnitude of these coefficients is treated as a function of the three variables describing the sky conditions. At this stage of model development, these are not continuous functions, but matrices corresponding to the discrete partition of the sky condition space presented above.

These coefficients constitute the statistical/experimental part of the model. They are obtained through the analysis of hourly—or higher fre-

Table 1. Description of the ϵ, Dh and θh intervals depicting the sky conditions

Dh (KJ/min)			ε			z (degrees)	
Name of Interval	Lower Bound	Upper Bound	Name of Interval	Lower Bound	Upper Bound	Lower Bound	Upper Bound
A	0	3	A	1	1	0	35
B	3	6	B	1.003	1.03	35	45
C	6	10	C	1.03	1.1	45	55
D	10	15	D	1.1	1.5	55	65
E	15	20	E	1.5	2.5	65	90
F	20	--	F	2.5	5		
			G	5	9		
			H	9	--		

quency—data recorded with ground-shielded pyranometers of different slopes and orientations. In order not to bias the model in favor of a specific orientation, measurements are needed in the four cardinal directions. Also, as this type of model is used primarily for sun-facing captors, one or more sloping, south-facing or sun-tracking measurements are needed.

The analysis consists of optimizing F_1 and F_2 for each [θ, ε, Dh] interval by least square fitting of measured data.

2.2 *Data sets*

Data from Trappes and Carpentras, France[12]; San Antonio, Texas[13]; and Albany, New York [14] are used in this analysis. These sites represent four distinct solar environments with latitudes ranging from 30° to 48°N and climates ranging from semi-arid subtropical to temperate marine. Table 2 summarizes the geographical and climatological particularities of each station.

The selected sites had to meet the three criteria presented below:

(1) *Availability of high quality hourly measurements of horizontal global and direct and/or diffuse irradiance, as well as tilted global irradiance for four azimuths*. The type of instrumentation used and the level of quality control achieved at the two leading Meteorologie Nationale stations, and two of the U.S. Solar Energy Meteorological Research and Training Sites, ensures the data quality needed for a study of this nature. Table 3 summarizes the measurements performed and instrumentation used at each site.

Table 2. Description of selected sites

Station	Latitude	Longitude	Elevation	Climate Type
Albany, New York	42° 42'N	73° 50'W	94m	Humid Continental Temperate
San Antonio, Texas	29° 46'N	98° 49'W	253m	Semi-arid Sub tropical
Carpentras, France	44° 05'N	5° 03'E	99m	Mediterranean
Trappes, France	48° 46'N	2° 0'E	167m	Marine Temperate

Table 3. Type of measurements used from each site and instrumentation

Station(s)**	Measurements(s)	Instrument
T,C,A,S	Direct irradiance	Eppley NIPS
T,C,A,S	Global irradiance	Thermal pyranometers*
T,C	South, west, east and north vertical global irradiance	Thermal pyranometers*
S	South, west, east and north ground-shielded vertical global irradiance	Thermal pyranometers*
A	South, west, east and north ground-shielded vertical global irradiance	Li-Cor filtered radiometers
T,C	45° tilt, south facing global irradiance	Thermal pyranometers*
A,S	Latitude, latitude +10° and latitude -10° tilt south facing, ground shielded global irradiance	Thermal pyranometers*
T,C	North and south vertical reflected radiation. Sky shielded instruments.	Thermal pyranometers*

NOTES: * Both Kipp and Zonen CM5 and Eppley PSPs are used at the French stations. The American sites used only Eppley PSPs

** A: Albany; C: Carpentras; S: San Antonio; T: Trappes

(2) *Elimination of most assumptions regarding ground-reflected radiation*. In order to focus on sky radiance distribution, assumptions regarding directionality of ground-reflected radiation and albedo must be minimized.

Tilting pyranometers from the two American sites are equipped with artificial horizons (cylindrical black-painted shields for Albany, and planar black-painted shields for San Antonio). The two French stations provide independent records of ground reflected radiation measured with sky-shielded vertically mounted pyranometers facing north and south. Ground-reflected iradiance is removed from east and west vertical sensors by assuming that it is equal to the half sum of the north and south vertical reflected irradiances. Further, the ground component is removed from the 45° south facing sensor by assuming isotropy of the south-reflected component.

(3) *Availability of at least three seasonally representative months of hourly data*. This criteria allows notably for analysis of a given site under three typical solar geometry configuration.

Albany data includes the months of February, April, and June 1980, (out of the four years available), while San Antonio data includes December 1980, March, July, and December of 1981. Data from Trappes cover a 21-month period starting in April 1979, while Carpentras data cover a two-year period (Jan. 1979 to Dec. 1980).

In addition to the four hourly data bases described above, one-minute data from Albany, NY covering the months of February, April and June 1980 are used to study the model on a short time interval basis.

2.3 *Model testing, reference models*

The model's performance is observed from three different viewpoints: (1) dependent tests, (2) independent tests, and (3) real time performance.

2.3.1 *Dependent tests*. The enhancement matrices F_1 and F_2 are established for each station as explained earlier. The completed models are then tested against the data sets used for their establishment.

For each available sensor orientation, the mean bias error (MBE) and the root mean square error (RMSE), accumulated over the complete testing period at each station, are used to rate model performance.

The goal of these dependent tests is to evaluate the limits of the Perez model configuration ability to recreate existing conditions.

2.3.2 *Independent tests*. The Albany-established model is now tested against data from the three other sites. As above, MBE and RMSE cor-

responding to the complete testing period for each site are used to rate performance.

The question of site/climate dependency of the sky condition description method used is answered to a large extent by these tests.

2.3.3 *Real time tests*. Based on the Albany one-minute data set, the model's behavior is observed in real time for typical weather conditions, such as winter/summer clear days, winter/summer thin overcast days and winter/summer partly cloudy days.

2.3.4 *Reference models*. Three models are used as reference to provide an objective comparative basis to all the above tests. These are the following: (1) The isotropic (Liu and Jordan[15]) model, (2) The Hay model[6] and, (3) The Klucher model[7]. The latter models were selected as they had been found to operate generally better than the isotropic and several other models, e.g. [16].

The Klucher model is based on the Temps and Coulson[17] clear sky equation. This was designed to incorporate both the observed horizon and circumsolar brightening in the computation of energy impinging on slopes. The governing equation is

$$Dc = Dh(1 + \cos s)/2\{1 + F \sin^3(s/2)\} \times \{1 + F \cos^2 \theta \sin^3 z\}, \quad (11)$$

where F is used to parameterize the sky condition and is given by,

$$F = 1 - (Dh/Gh)^2, \quad (12)$$

where Gh is the horizontal global irradiance.

The Hay model incorporates only circumsolar brightening in its structure. As for Klucher's, the sky condition is depicted by one term expressing the amount of direct irradiance received at the earth surface. This clearness index term is given by,

$$K = I/I_o, \quad (13)$$

where I_o is the extraterrestrial radiation. The model's governing equation is,

$$Dc = Dh\{(K \cos \theta/\cos z) + (1 - K)(1 + \cos s)/2\}. \quad (14)$$

Both Klucher and Hay models return to an isotropic configuration in the absence of direct sunlight.

3. RESULTS

3.1 *Model's parameters establishment*

As an example of the complete analysis of each data set as described in Section 2.1.2, the variations of F_1 and F_2 with the two radiative quantities describing the sky conditions are plotted on Fig. 2(a) through 2(d) for the stations of Trappes, Carpentras, Albany and San Antonio, respectively, for solar zenith angles lying between 55° and 65°.

The scale on the Dh axis is linear, while that on the ϵ axis is logarithmic. No point was plotted if less than five hourly events were observed within a given [Dh, ε, z] category.

The most evident feature of these plots is their similarity: For four sets of independent data, the same type of pattern may be observed for F_1 and F_2. This includes the following:

- Increase in circumsolar brightening (F_1) with Dh for low ε values, (low direct radiation, bright atmosphere).
- Existence of both circumsolar and horizon brightening (F_1 and F_2) as ε increases, with increased relative horizon contribution when approaching very clear conditions (Low Dh, high ε). This is particularly visible on Fig. 3.
- Evidence of continuity between overcast and clear sky conditions indicating the persistence of a specific pattern for all intermediate cases (e.g., broken clouds).
- Tendency toward isotropic configuration for dark overcast atmospheres.

Disparities may also be noted between the four plots. The most interesting pertains to the relative importance of horizon brightening for clear atmospheres: this is maximum for the San Antonio, Texas station, and the Carpentras station, while horizon contribution is comparatively lower for Trappes and Albany. The effect of both climate/geography and instrumentation are discussed in the next section. However, it is interesting to note that (1) the station at the highest elevation exhibits the most brightening at the horizon; (2) the two driest stations, exhibiting the largest number of clear atmosphere events, also show the most pronounced horizon brightening—compare for example Figs. 4(a) (Trappes) and 4(b) (Carpentras) where the number of hourly events in each [Dh, ε] is reported for the studied solar zenith angle range; (3) the regions of San Antonio and Carpentras, due to their dry climate, have the least amount of green vegetation, and consequently the highest albedo.

3.2 *Model performance*

3.2.1 *Long-term tests*. Tables 4(a) through 4(d) summarize the overall results obtained by testing models against each complete data set. These show for Trappes, Carpentras, Albany and San Antonio respectively, (1) the average hourly energy, Gc, received by each sloping sensor; (2) the root mean square error obtained for each model in terms of percentage of the previous value; and (3) the mean bias error for each model, also in percent.

Each table contains tests results for the three reference models, the new model using Albany-derived parameters (i.e., independent test), and the new model using each station's derived parameters (i.e., dependent tests).

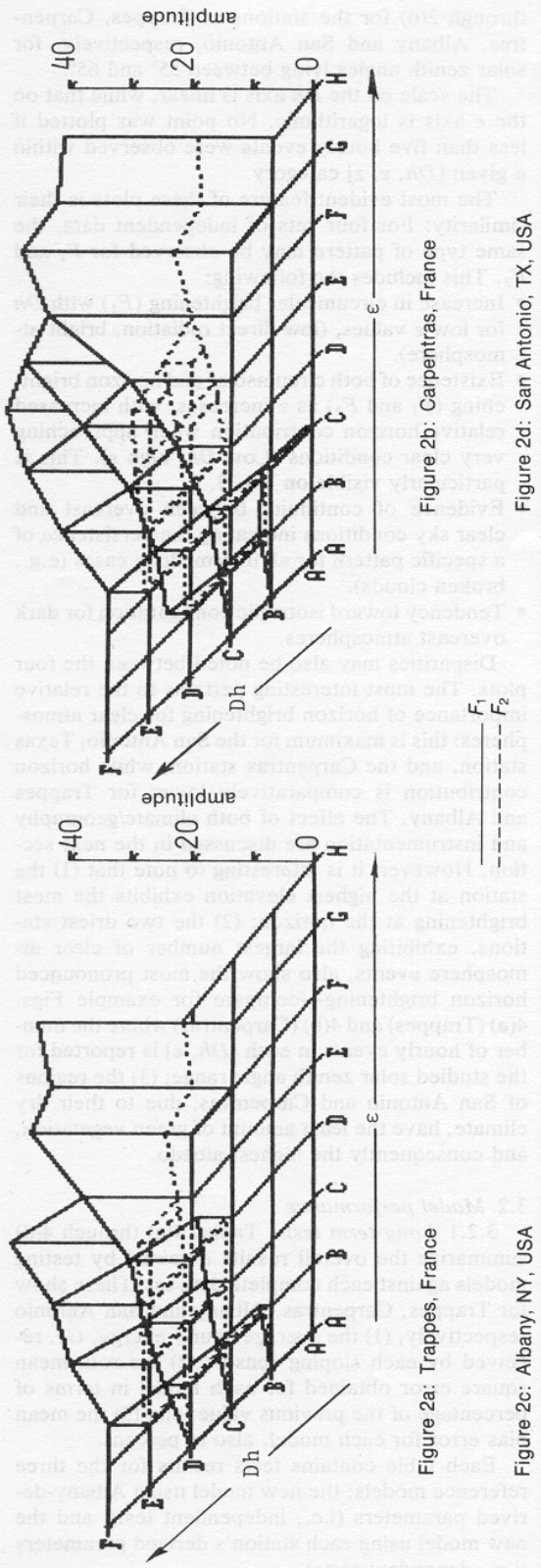

Figure 2a: Trappes, France

Figure 2b: Carpentras, France

Figure 2c: Albany, NY, USA

Figure 2d: San Antonio, TX, USA

Fig. 2. Variations of circumsolar brightening coefficient, F_1 (solid lines) and horizon brightening, F_2 (dotted lines) with Dh and ε, for $55° < z < 65°$.

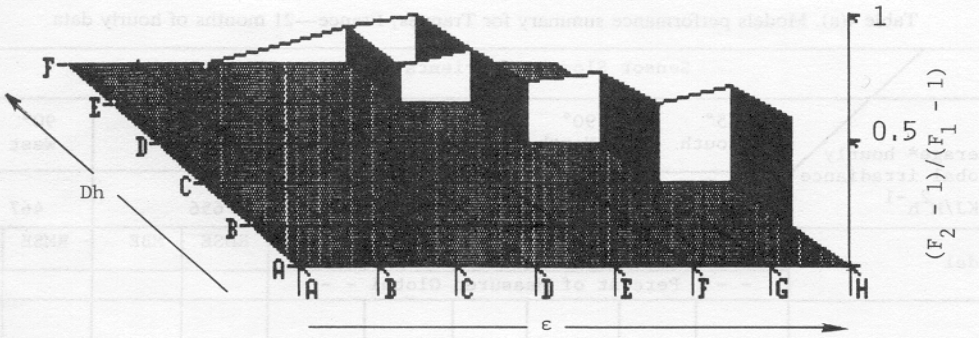

Fig. 3. Variation of the relative magnitudes of horizon and circumsolar brightening with *Dh* and ε for $55° < z < 65°$.

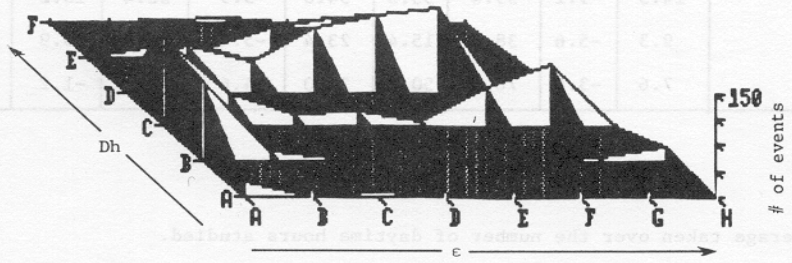

(a)

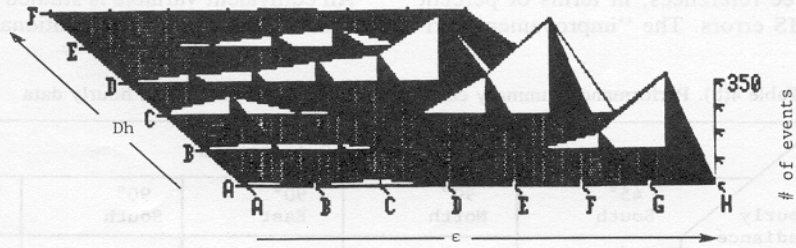

(b)

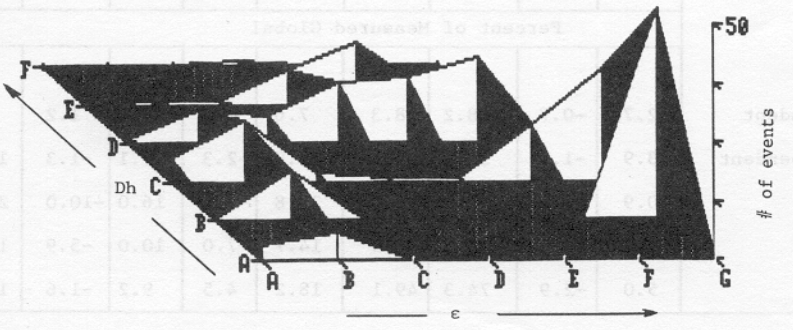

(c)

Fig. 4. Number of hourly events analyzed in each [*Dh*, ε] interval for $55° < z < 65°$; (a) Trappes—21 months of data; (b) Carpentras—24 months of data; (c) Albany—3 months of data.

Table 4(a). Models performance summary for Trappes, France—21 months of hourly data

Sensor Slope and Orientation										
Average* hourly global irradiance KJ/M^2h^{-1}	45° South		90° North		90° East		90° South		90° West	
	1060		234		520		656		467	
Model	RMSE	MBE	RMSE	MBE	RMSE	MBE	RMSE	MBE	RMSE	MBE
	- - Percent of Measured Global - -									
Perez dependent	5.1	-0.4	18.2	7.6	12.9	-1.3	10.2	2.3	14.1	5.4
Perez independent	5.7	-1.2	23.9	14.0	14.4	-1.0	10.4	1.3	15.6	5.9
Isotropic	14.3	-9.1	53.4	33.3	34.0	-5.9	22.4	-10.2	31.2	0.4
Hay	9.3	-5.6	38.0	15.4	23.4	-5.4	14.9	-5.9	21.4	0.1
Klucher	7.6	-3.6	76.5	50.8	30.0	4.6	14.2	-1.2	32.1	12.0

Note: * Average taken over the number of daytime hours studied.

Table 5 summarizes, for each station and sensor orientation, and for independent testing, the improvement achieved with the proposed model over each of the three references, in terms of percent decrease of RMS errors. The "improvement variable," X, is defined as,

$$X = 100(1 - \text{RMSE Perez/RMSE Reference}) \quad (15)$$

An equivalent variable is studied in Table 6, but this time it represents the additional improvement

Table 4(b). Performance summary carpentras, France—24 months of hourly data

Sensor Slope and Orientation										
Average* hourly global irradiance KJ/M^2h^{-1}	45° South		90° North		90° East		90° South		90° West	
	1574		230		687		972		715	
Model	RMSE	MBE	RMSE	MBE	RMSE	MBE	RMSE	MBE	RMSE	MBE
	Percent of Measured Global									
Perez dependent	2.7	-0.7	18.2	8.3	7.6	0.6	5.7	1.2	7.0	0.5
Perez independent	3.9	-1.8	30.0	0.1	10.9	-2.3	7.1	-1.3	10.2	-2.4
Isotropic	10.9	-7.8	47.8	24.0	20.8	-6.9	16.0	-10.0	21.4	-7.7
Hay	6.0	-4.2	36.9	-6.5	14.7	-7.0	10.0	-5.9	14.0	-7.1
Klucher	5.0	-2.9	74.3	49.1	18.2	4.5	9.2	-1.6	18.0	3.2

Note: * Average taken over the number of daytime hours studied

Table 4(c). Performance summary Albany, New York, USA—3 months of hourly data

Average* hourly global irradiance KJ/M^{2}h^{-1}	Sensor Slope and Orientation: 43° South		90° North		90° East		90° South		90° West	
	1401		260		661		781		617	
Model	RMSE	MBE	RMSE	MBE	RMSE	MBE	RMSE	MBE	RMSE	MBE
	Percent of Measured Global									
Perez dependent	2.9	-0.2	12.7	4.2	8.2	-1.1	6.5	1.6	9.4	0.2
Isotropic	8.9	-5.6	37.7	18.8	26.0	-6.2	15.9	-6.6	27.0	-5.7
Hay	5.6	-3.3	30.4	-3.8	16.5	-7.0	10.5	-4.9	18.3	-7.4
Klucher	4.1	-1.5	60.0	-38.8	22.5	3.9	10.7	-1.8	24.3	5.0

Note: * Average taken over the number of daytime hours studied

achievable when a dependent test is performed. This variable, Y, is given by,

$$Y = 100(1 - \text{RMSE Perez Dependent}/\text{RMSE Perez Independent}) \quad (16)$$

It is interesting to note, as in Section 3.1, that the largest improvement is found for the two stations which have the most different climatic and geographical environments compared to Albany, NY.

3.2.2 *Real time performance*. The difference between measured and modeled radiation values is plotted for selected orientations against time of day for five typical insolation conditions encountered

Table 4(d). Performance summary San Antonio, Texas, USA—4 months of hourly data

Average* hourly global irradiance KJ/M^{2}h^{-1}	Sensor Slope and Orientation: 30° South		90° North		90° East		90° South		90° West	
	1946		216		771		1523		884	
Model	RMSE	MBE	RMSE	MBE	RMSE	MBE	RMSE	MBE	RMSE	MBE
	Percent of Measured Global									
Perez dependent	2.2	0.5	19.4	8.8	6.7	-1.6	4.6	-2.2	4.9	0.3
Perez independent	2.1	-0.3	26.4	-15.7	10.9	-7.4	7.0	-5.0	8.0	-5.3
Isotropic	5.9	-4.6	33.3	-10.6	21.7	-13.7	16.3	-13.3	19.2	-12.8
Hay	3.0	-1.6	56.0	-40.3	18.9	-14.8	10.8	-8.9	15.2	-11.8
Klucher	2.6	-1.0	39.8	9.3	15.7	-6.6	11.0	-8.4	13.0	-5.9

Note: * Average taken over the number of daytime hours studied

in Albany, New York. The solid lines correspond to the isotropic model, while Klucher, Hay, and Perez models are represented by x-lines, $+$-lines and o-lines respectively.

Figures 5(a), (b), and (c) illustrate the case of a winter clear day (February 4, 1980) for the 43° south, the east vertical and north vertical surfaces. Winter, thin overcast conditions, prevailed on February 3, 1980. Results are plotted on Figs. 6(a) and (b) for the 53° south and the north sensors respectively. Figures 7(a) and (b) illustrate variable conditions with several clear occurrences in the morning (February 13, 1980); results are shown for the vertical south and north surfaces, respectively.

The cases of a clear summer day and a high turbidity hazy summer day are illustrated by Figs. 8(a)

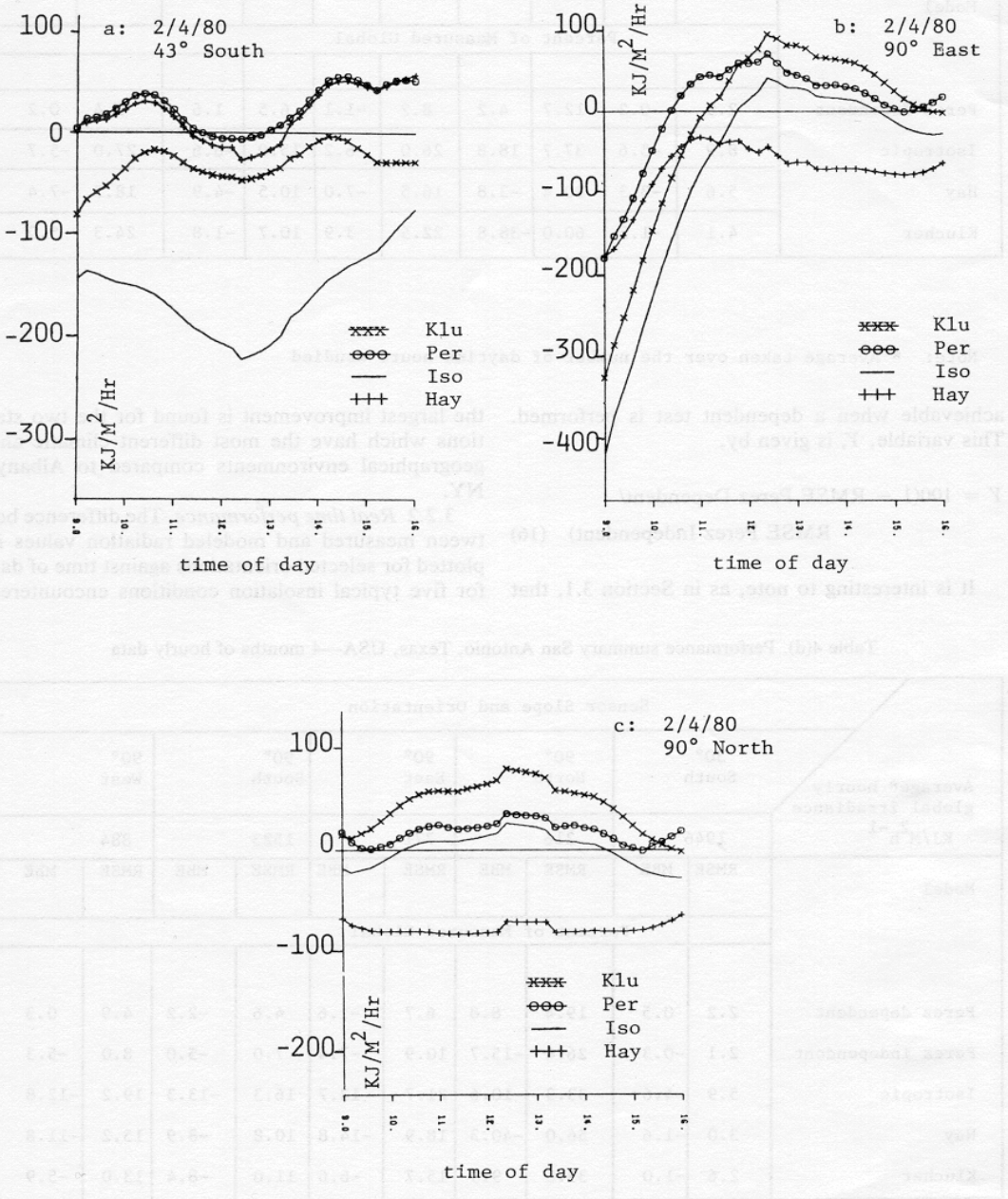

Fig. 5. Daily variations of the difference between modeled and measured irradiance values on a clear, winter day, based on one-minute data in Albany, NY, February 4, 1980.

Table 5. Percent reduction of RMS error, using the proposed model for independent tests: (1 − (RMSE Perez independent)(RMSE Reference Model)$^{-1}$) × 100

	Sensor Slope and Orientation														
	Sloping* South			90 degs. North			90 degs. East			90 degs. South			90 degs. West		
Reference	Iso	Hay	Klu	Iso	Hay	Klu	Iso	Hay	Klu	Iso	Hay	Klu	Iso	Hay	Klu
Albany	67%	48%	29%	66%	58%	79%	68%	50%	66%	59%	38%	39%	65%	49%	61%
Trappes	61%	39%	25%	56%	37%	64%	58%	39%	52%	54%	31%	27%	51%	27%	51%
Carpentras	65%	36%	23%	45%	28%	64%	48%	26%	40%	56%	29%	22%	53%	27%	43%
San Antonio	65%	33%	24%	27%	46%	37%	44%	35%	30%	58%	29%	39%	51%	41%	30%

Note: All tests are independent but for Albany, NY

* 45° for Trappes and Carpentras, 43° for Albany, 30° for San Antonio

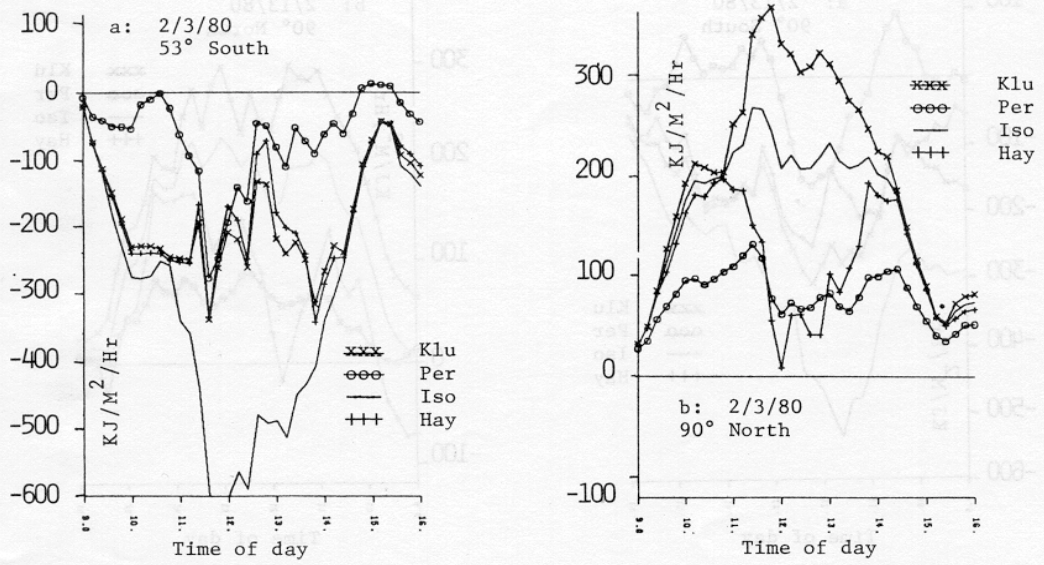

Fig. 6. Daily variations of modeled minus measured irradiance on a thin overcast, winter day based on February 3, 1980 one-minute data, in Albany, NY.

Table 6. Additional percent reduction of RMS error using station-derived model: (1 − (RMSE Perez dependent)(RMSE Perez Independent)$^{-1}$) × 100

Station	Sensor Slope and Orientation				
	Sloping* South	90° North	90° East	90° South	90° West
Trappes	11%	23%	11%	1%	10%
Carpentras	30%	31%	30%	20%	30%
San Antonio	0%	27%	37%	28%	39%

* 45°, Trappes and Carpentras, 43°. Albany, 30°, San Antonio

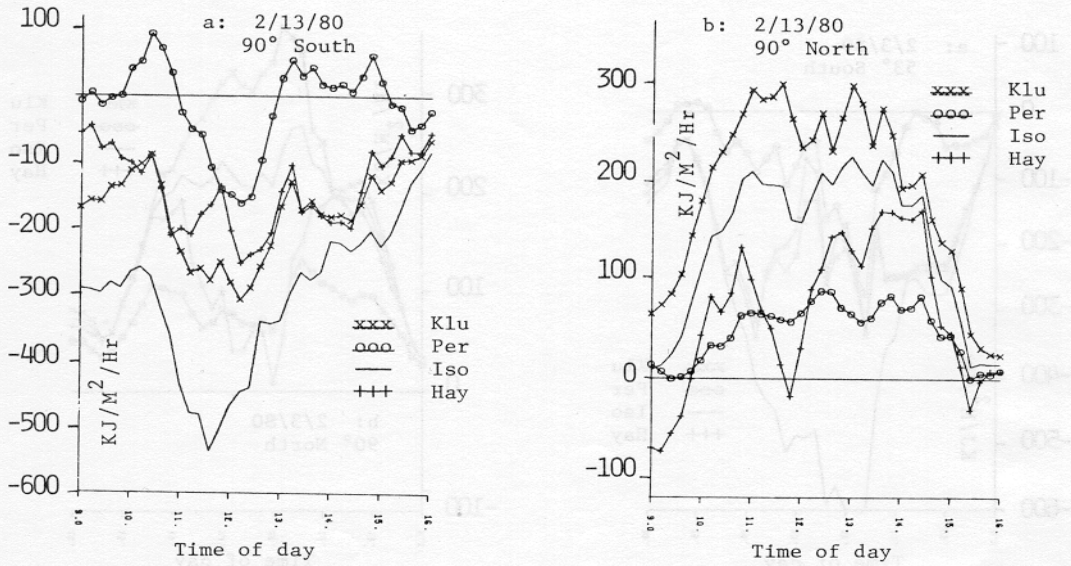

Fig. 7. Daily variations of modeled minus measured irradiance on a mixed cloudy winter day based on February 13, 1980 one-minute data in Albany, NY.

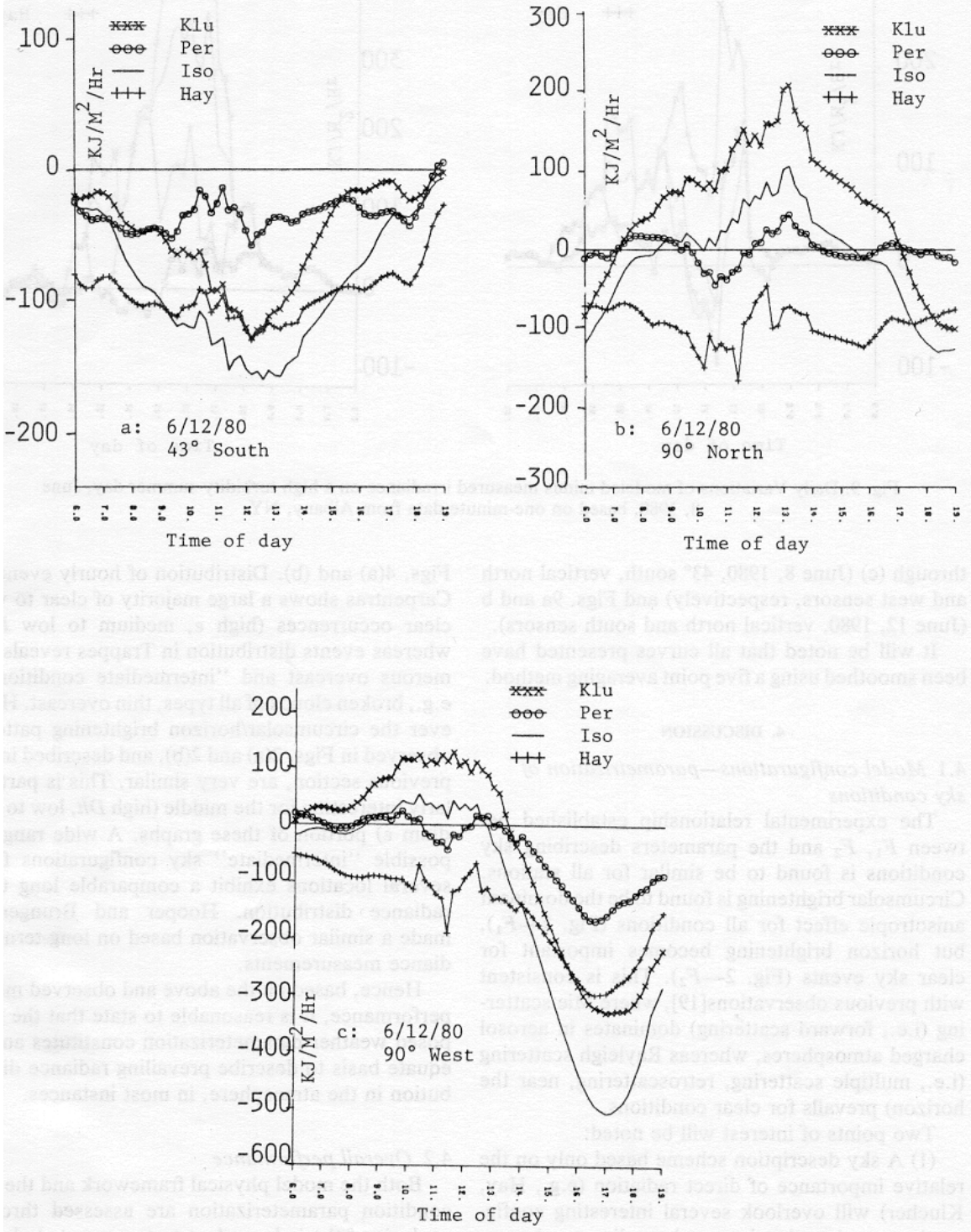

Fig. 8. Daily variations of modeled minus measured irradiance on a clear summer day, based on June 12, 1980 one-minute data in Albany, NY.

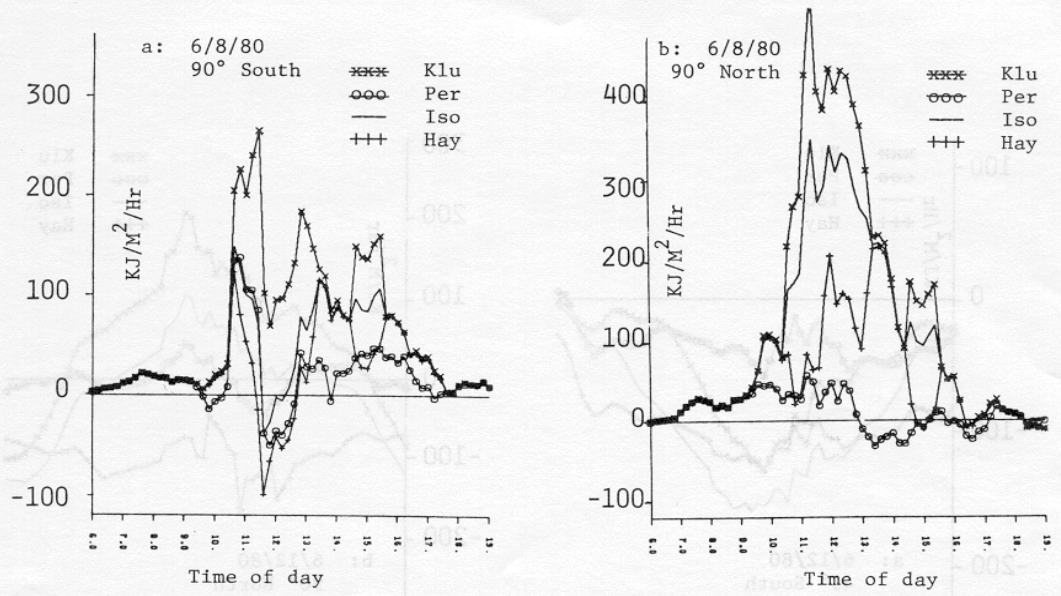

Fig. 9. Daily Variations of modeled minus measured irradiance on a high turbidity summer day, June 8, 1980, based on one-minute data from Albany, NY.

through (c) (June 8, 1980, 43° south, vertical north and west sensors, respectively) and Figs. 9a and b (June 12, 1980, vertical north and south sensors).

It will be noted that all curves presented have been smoothed using a five point averaging method.

4. DISCUSSION

4.1 *Model configurations—parametrization of sky conditions*

The experimental relationship established between F_1, F_2 and the parameters describing sky conditions is found to be similar for all stations. Circumsolar brightening is found to be the dominant anisotropic effect for all conditions (Fig. 2—F_1), but horizon brightening becomes important for clear sky events (Fig. 2—F_2). This is consistent with previous observations[19], where Mie scattering (i.e., forward scattering) dominates in aerosol charged atmospheres, whereas Rayleigh scattering (i.e., multiple scattering, retroscattering, near the horizon) prevails for clear conditions.

Two points of interest will be noted:

(1) A sky description scheme based only on the relative importance of direct radiation (e.g., Hay, Klucher) will overlook several interesting configurations, such as the circumsolar radiance enhancement observed for bright atmospheres where there is no or little direct beam (high Dh, low ε).

(2) The proposed (Dh, ε) grid appears to account globally for most "intermediate" sky configurations. This is best seen through the following example:

The climatic difference between the stations of Trappes and Carpentras is obvious when comparing Figs. 4(a) and (b). Distribution of hourly events in Carpentras shows a large majority of clear to very clear occurrences (high ε, medium to low Dh), whereas events distribution in Trappes reveals numerous overcast and "intermediate conditions," e.g., broken clouds of all types, thin overcast. However the circumsolar/horizon brightening patterns observed in Figs. 2(a) and 2(b), and described in the previous section, are very similar. This is particularly interesting for the middle (high Dh, low to medium ε) portion of these graphs. A wide range of possible "intermediate" sky configurations from several locations exhibit a comparable long term radiance distribution. Hooper and Brunger[20] made a similar observation based on long-term radiance measurements.

Hence, based on the above and observed model performance, it is reasonable to state that the proposed weather parameterization constitutes an adequate basis to describe prevailing radiance distribution in the atmosphere, in most instances.

4.2 *Overall performance*

Both the model physical framework and the sky condition parameterization are assessed through analysis of the independent tests presented above. Performance against ground-shielded data from three widely different solar environments show that they both constitute an adequate approach to the modelization of irradiance on a slope.

Indeed, after fair testing, substantial performance improvement over existing anisotropic models is found for all orientations and all stations when using the RMS error as a standard (Table 5). Per-

formance improvement based on MB error is also remarkable for almost all stations and sensor orientations.

4.3 *Site/climate dependency*

Site dependency is not found in the first approach to be a major stumbling block for the model. However, the F_1/F_2 pattern differences between stations, and the margin for performance improvement from independent to dependent testing are certainly worth additional investigation.

Two possible causes had been originally advanced[8] to explain performance and model configuration differences between sites. These are the following: (1) Climatical/geographical reasons and (2) instrumentation differences. It appears at this point that the influence of the latter is secondary because of the following reasons:

(a) As the most sensitive instrumentation difference between sites is the method for excluding ground-reflection, variations in the quantity of horizon brightening observable for each site should be explained on this basis. However, Trappes and Albany, where two opposite methods for removing ground-reflected irradiance are used—sky shields vs ground shields—exhibit very similar patterns for horizon brightening. Nevertheless, a more complete investigation (e.g., side by side comparison) is needed to eliminate any doubts regarding this matter.

(b) Most observed differences can be logically associated with climatic/geographical differences. These are as follows:

(1) Clear sky horizon brightening is found to be the most pronounced for the highest station, San Antonio, Texas. Indeed, the multiple and retroscattering occurring near the horizon should play an increasing role as altitude increases and radiance from the top of the atmosphere decreases.

(2) Horizon brightening is found to be more intense for the two driest stations (Carpentras and San Antonio). The higher ground albedo associated with dry climate vegetation, and the resulting intensified retroscattering, could explain this observation.

(3) Performance improvement from an Albany-derived model to a station-derived model is larger when climatic differences are more pronounced (e.g., Trappes vs. Carpentras—compare climatic differences: Fig. 4(c) with Figs. 4(a) and 4(b).

The logical follow-up of this work is to analyze the model configuration obtained for a set of specific climate/altitude/environment stations, and to assess the validity of interpolation between sites.

4.4 *Performance vs. reference models—Perez model's limitations*

Real time analysis reveals specific points of interest, contrasting the Perez model's performance with that of the selected reference standards.

The first important point to be noted is that the isotropic model is inadequate for applications requiring dynamic simulations. This is best seen on February 3 for the south-facing 53° slope, where the error generated exceeds 600 JK/m^2/hr (35%) around noon time. It will be noted that an error of that magnitude will persist from sunrise to sunset for tracking flat plate collectors and would likely be increased for low concentrators.

The strength of the proposed design compared to the two anisotropic references is twofold:

(1) The weather condition parametrization includes both direct and diffuse radiation, treated as independent variables, rather than direct radiation only. This may be seen clearly on Fig. 6 to a lesser extent on Figs. 7 and 8. There was almost no direct radiation present on February 3 before 11 AM and after 2 PM, although diffuse radiation was intense. Only the proposed model differed noticeably from the isotropic configuration and could account for part of the existing anisotropy.

(2) This model can go from a circumsolar enhancement configuration to a circumsolar + horizon enhancement configuration depending on the type of sky condition, whereas the Hay model is purely circumsolar; and while the Klucher model includes both circumsolar and horizon brightening, the two terms are not allowed to vary independently. The lack of horizon brightening in the Hay model will cause it to underestimate on clear days for surfaces which do not face the sun (see Fig. 5(b), afternoon, Fig. 5(c) and Fig. 8(c)); it will also underestimate on clear days for all orientations when the zenith angle is small (see Figs. 8(a)–8(c)). On the other hand, the structure of the Klucher model is responsible for its tendency to overestimate for slopes that do not face the sun, particularly on high turbidity days when forward scattering is the only noticeable effect. This is particularly visible on Fig. 9(b) where the overestimate exceeds 100% between 11 AM and 12 PM.

It will also be noted that the Klucher model is bound by design to generate energy values larger than the isotropic values (this may be seen in all tables and daily plots). Additionally, there is a limit by which isotropic values can be exceeded by this model (this limit is equal to 2.7 for $F = 1$, $z = 90°$ and $\theta = 0°$). Consequently, it will not perform as well as either the Hay or the Perez model when directional scattering is very intense—see for example Fig. 5(b) between 9 AM and 11 AM.

The proposed design also reaches its limits, which are most apparent when looking at the real time plots, since there still exists some deviation between modeled and measured values. This performance limitation may be assessed by looking at dependent tests results on Tables 4(a)–4(d). The best achievable RMS errors over a long term period will typically be of the order of 11 to 18 Watts/m^2 for all orientations. Any improvement beyond this point would likely require a more complex ap-

proach to diffuse radiation modeling. However, it will be remarked that simple model design modifications presently under study have been observed to push that limitation another step further. This involves notably differential horizon brightening as a function of azimuth.

4.5 *Model status, developmental work in progress*

There are two points of interest which are now being investigated, or which will require additional work. These are the following:

(1) Establishment of a comprehensive climate/geography/environment/model configuration relationship, based on existing or new data bases at selected sites (e.g., based on classifications such as [19]), as well as investigation of potential site interpolations.

(2) Model design improvements, such as framework modifications as mentioned above, or sky condition parametization based on another combination of the three selected variables—notably, the use of z as dependent rather than independent variable will be investigated. Design improvements will be limited to those requiring no more input parameters than presently used. Also, model end-use simplifications will be investigated. These will noticeably include the use of analytical functions rather than three-dimensional matrices for the coefficients F_1 and F_2, as soon as final model configurations are obtained from extended data analysis.

CONCLUSION

The model, which has been presented, is based on three basic ideas: (1) a geometrical representation of the sky dome incorporating variable circumsolar and horizon atmosphere brightening, (2) a parametric description of the insolation conditions, based on available radiative quantities, and (3) an experimentally-derived law governing the variations of circumsolar and horizon brightening with the insolation conditions.

Model performance is found to be adequate when independently tested against hourly tilted irradiance data sets from Trappes and Carpentras, France, and San Antonio, Texas. Ground-reflected irradiance was either removed at the acquisition site, or independently measured, thereby eliminating assumptions on that matter. Results reveal a systematic performance improvement by this model over the isotropic model and the models of Hay and Klucher, which were used as references. The isotropic RMS errors are typically reduced by 40–60% while Hay's and Klucher's are typically reduced by 25–40% and 20–60%, respectively.

Within this study's context, site-dependency is not found to be a major stumbling block for either the insolation parametrization method or the model itself. This is quite apparent by looking both at the Albany derived model performance and at the similar experimentally-derived laws obtained from the two widely different climate environments of Trappes and Carpentras.

However, there exists a substantial margin for performance improvement, as demonstrated by the results of dependent model tests. These suggest that climate (hence vegetation) and altitude have an influence on the model's configuration and performance which can be interpreted on a deterministic basis. A systematic analysis of their influence, involving several climate/altitude pilot sites will certainly be worth the effort, as typical long-term RMS error could be reduced down to about 15 Wm^{-2} for fixed surfaces of any orientations. This performance improvement is likely to be even more noticeable when considering tracking flat plate or low concentration captors.

Acknowledgement—This work was supported by USDOE contract #DEFG0577ET20182 and by the Atmospheric Sciences Research Center's Energy Group.

REFERENCES

1. IEA Solar Heating and Cooling Programme, Task IX Solar radiation and pyranometry studies. International Energy Agency, Paris, France.
2. C. C. Y. Ma and M. Iqbal, Statistical comparison of models for estimating solar radiation on inclined surfaces. *Proc. of ASES*, Minneapolis, Minnesota, 871 (1983).
3. P. S. Lunde, Prediction of the performance of solar heating systems utilizing annual storage. *Solar Energy*, **22,** 69 (1979).
4. D. Menicucci and Fernandez, Verification of Photovoltaic System modeling codes based on system experimental data. *Proc.* XVII*th IEE Photovoltaic Specialists Conference*, Kissimmee, Fla. (1984).
5. V. M. Puri, R. Jimenez and M. Menzer, Total and non-isotropic diffuse insolation on tilted surfaces. *Solar Energy* **25,** 85 (1980).
6. J. E. Hay and J. A. Davies, Calculation of the the solar radiation incident on an inclined surface. *Proc.* 1*st Canadian Solar Radiation Data Workshop*. J. E. Hay and T. K. Won, Toronto, pp. 59–72 (1980).
7. T. M. Klucher, Evaluation of models to predict insolation on tilted surfaces. *Solar Energy*, **23,** 111 (1978).
8. R. Stewart and R. Perez, Validation of an anisotropic model estimating insolation on Tilted Surfaces. Proc. of ASES, Anaheim, California, 639–644 (1984).
9. R. R. Perez, J. T. Scott and R. Stewart, An anisotropic model for diffuse radiation incident on slopes of different orientations, and possible applications to CPCs. *Proc. of ASES*, Minneapolis, Minnesota, 883–888 (1983).
10. M. Kano, Effect of a turbid layer on Radiation Emerging from a Planetary Atmosphere. Doctoral Dissertation, University of California, Los Angeles (1964).
11. A. Zelenka, Personal Communication, Swiss Meteorological Institute, Zurich, Switzerland (1984).
12. Direction de la Meteorologie, Service Meteorologique Metropolitain, Stations #260 (Trappes) and 874 (Carpentras), Paris, France.
13. Solar Energy Meteorological Research and Training Site Region V, San Antonio, Texas (1981).
14. Solar Energy Meteorological Research and Training Site Region II, Albany, New York (1980).

15. B. Y. H. Liu and R. C. Jordan, The interrelationship and characteristic distribution of direct, diffuse and total solar radiation. *Solar Energy*, **4,** 1 (1960).
16. A. Lebru, Cahier du CSTB 1847, #239. Centre Scientifique et Technique du Batiment, SophiaAntipolis, France (1983).
17. R. C. Temps and K. L. Coulson, Solar radiation incident upon slopes of different orientations, *Solar Energy*, **19,** 179 (1977).
18. K. L. Coulson, *Solar and Terrestrial Radiation*, pp. 84–100. Academic Press, New York (1975).
19. R. C. Callino and M. S. Vojtesak, Solar Climates of the United States based on Long-Term monthly averaged daily insolation values, *Solar Energy* **31,** 283 (1983).
20. M. A. Rosen, F. C. Hooper and A. P. Brunger, The characterization and modelling of the diffuse sky radiance. *Proc. of ISES*, Montreal, Canada (1985).